10-1-2007

Thin-Film Evolution Equation for a Strained Solid Film on a Deformable Substrate: Numerical Steady States

Wondimu T. Tekalign
Rochester Institute of Technology

Brian J. Spencer
University at Buffalo

Recommended Citation
W.T. Tekalign and B.J. Spencer, Journal of Applied Physics 102, 073503 (2007). https://doi.org/10.1063/1.2785024

Journal of Applied Physics, 1 October 2007
J. Appl. Phys. **102**, 073503 (2007) *(7 pages)*

Up: Issue Table of Contents
Go to: Previous Article | Next Article
Other formats: HTML (smaller files) | PDF (725 kB)

Thin-film evolution equation for a strained solid film on a deformable substrate: Numerical steady states

W. T. Tekalign*

School of Mathematical Sciences, Rochester Institute of Technology, 85 Lomb Memorial Drive, Rochester, New York 14623, USA

B. J. Spencer

Department of Mathematics, University at Buffalo, Buffalo, New York 14260, USA

(Received: 15 May 2007; accepted: 6 August 2007; published online: 1 October 2007)

We consider the nonlinear behavior of the thin-film evolution equation for a strained solid film on a substrate. The evolution equation describes morphological changes to the film by surface diffusion in response to elastic energy, surface energy, and wetting energy. Due to the thin-film approximation, the elastic response of the film is determined analytically, resulting in a self-contained evolution equation which does not require separate numerical solution of the full three-dimensional elasticity problem. Using a pseudospectral predictor-corrector method we numerically determine the family of steady state solutions to this evolution equation which correspond to quantum dot and quantum ridge morphologies. ©2007 *American Institute of Physics*

Contents

INTRODUCTION

Spontaneously formed periodic domain structures of nanoscale islands (quantum dots) in epitaxially strained thin solid films

have become a subject of intense theoretical and experimental study. These islands have unique optical, electronic and magnetic properties which signifies their importance in quantum dot applications.[1,2] These islands are small (a few nanometers) in size and hence difficult to prepare by standard lithographic techniques. One promising way is the formation of islands by a Stranski-Krastanow growth process, whereby the planar film undergoes a morphological instability.[3,4,5,6] During heteroepitaxial growth, the instability of surfaces under strain and subsequent island formation is caused by the competition between the surface free energy and the strain energy of the system.[7,8,9,10,11]

In experimental study of the nonlinear evolution of the stress driven instability of thick films the formation of deep, cusplike grooves was observed.[12,13] In Ref. 14 this instability was studied numerically and they showed that the surface instability creates a groove that sharpens as it grows deeper. In Ref. 15 a fully nonlinear bifurcation analysis was performed and by tracking the branch of steady state solutions numerically they found that the steady state solution branch terminates as the solutions form a cusp singularity.

In a thin film, however, cusp formation is suppressed as the surface approaches the film substrate interface. The different stress fields and the different surface energies of the film and the substrate affect the surface morphology, and the film-substrate interface is prevented from being exposed when the wetting criterion is satisfied. Stranski-Krastanow islands will be formed in this case.[16] The steady states of island shapes were studied by many researchers.[17,18,19,20,21,22]

While the understanding of some of the theoretical and modeling issues is well developed, the implementation of the models as large-scale numerical simulations is not yet feasible. The central issue is that the dynamics of the surface morphology are coupled to the elastic strain in the system, so dynamic models require solving the elasticity problems throughout the film and substrate at each time step and are limited by storage limitations for three-dimensional problem. Simulations involving the full elasticity problem are limited to one or few islands.[23] Only one recent work[24] explored a large number of islands using a large-scale three-dimensional calculation. This work uses the same elastic constants for both the film and the substrate. In Ref. 25 the evolution of a large number of islands was obtained using small slope approximation on a rigid substrate.

In Ref. 26 we developed an approximate solution to the elasticity problem which is valid when the film is thin. This elasticity solution is valid for arbitrary elastic constants in the film and substrate. The resulting elasticity solution then removes the necessity for solving the full three-dimensional elasticity problem numerically, and may provide a means for implementing large-scale simulations. Our work here is to apply numerical methods to the evolution equation to study the formation of islands. Within this framework, in Ref. 29 a nonlinear evolution equation with a second-order approximation for the stress field and a nonlinear wetting potential for the interface was considered, and it was claimed that the combined effect of nonlinear stress and wetting can terminate the coarsening process and lead to the formation of arrays of equal-sized islands. Levine *et al.*[30] found that wetting interaction can damp the long-wave perturbations and lead to Turing-type instability, further a weakly nonlinear analysis showed a possibility for spatially periodic arrays of quantum dots which are unstable.

The rest of the paper is organized as follows. In Sec. II we present the full nonlinear model for morphological evolution in thin solid films. In Sec. III we present the thin-film scalings and the thin-film evolution equation. In Sec. IV we present the numerical method used, and in Sec. V we characterize the steady state island-like solutions. Finally in Sec. VI we summarize our results.

MODEL FOR FILM GROWTH

We begin with the model from Ref. 6 for the growth of a single-component epitaxial film on a substrate. We specialize the model to describe the annealing of a film (no vapor deposition). The film lies in $0<z<h(x,y,t)$, the vapor in $z>h(x,y,t)$, and the substrate occupies $z<0$. The vapor is taken to be at zero pressure and the stress in the film and the substrate are governed by isotropic linear elasticity,

$$\sigma_{ij} = \frac{2\mu\nu}{1-2\nu}\delta_{ij}E_{kk} + 2\mu E_{ij}, \qquad (1)$$

where μ is the elastic shear modulus, ν is the Poisson ratio, δ_{ij} is the Kronecker delta, and E_{ij} is the linear elasticity strain

tensor given by

$$E_{ij} = \frac{1}{2}(\partial_i u_j + \partial_j u_i). \qquad (2)$$

Here u_i is the ith Cartesian component of the displacement vector, where the index i=1,2,3 corresponds to the x,y,z coordinates, respectively, and ∂_j indicates partial derivative with respect to the jth coordinate. Repeated indices imply summation from 1 to 3. The quantities u_i, σ_{ij}, E_{ij}, μ, and ν are defined separately in the film (F) and substrate (S). Since mechanical equilibrium exists within the film and the substrate,

$$\partial_j \sigma_{ij} = 0 \text{ in } F \text{ and } S. \qquad (3)$$

Upon substituting the formulas for stress and strain in these equation, we obtain Navier's equations for the equilibrium displacements,

$$(1-2\nu)\partial_k^2 u_i + \partial_k \partial_i u_k = 0 \text{ in } F \text{ and } S. \qquad (4)$$

On z=h(x,y,t) the force on the film surface (the traction in the direction of the normal $\hat{\boldsymbol{n}}$) is equal to the pressure in the vapor,

$$\sigma_{ij}^F \hat{n}_j = 0 \text{ on } z = h(x,y,t), \qquad (5)$$

where

$$\hat{n} = \frac{(-h_x, -h_y, 1)}{\sqrt{1+h_x^2+h_y^2}}. \qquad (6)$$

The substrate is taken to be semi-infinite, and so the displacements vanish far beneath the film,

$$u_i^S \to 0 \text{ as } z \to -\infty. \qquad (7)$$

Finally on z=0 (the film/substrate interface), the misfit condition gives

$$u_i^F = u_i^S + \epsilon \begin{bmatrix} x \\ y \\ 0 \end{bmatrix} \text{ on } z = 0, \qquad (8)$$

where ϵ is the misfit of the film, and the continuity of normal traction gives

$$\sigma_{ij}^F \hat{z} = \sigma_{ij}^S \hat{z} \text{ on } z = 0, \qquad (9)$$

where $\hat{\boldsymbol{z}}$ is the unit vector in the z direction.

The evolution equation is determined by surface diffusion in response to a chemical potential ψ according to[27]

$$\frac{\partial h}{\partial t} = D\sqrt{1+|\nabla h|^2}\nabla_S^2(\psi), \qquad (10)$$

where ∇_S^2 is the surface Laplacian,

$$\nabla_S^2 = \frac{1}{1+h_x^2+h_y^2}\left[(1+h_y^2)\partial_x^2 - 2h_xh_y\partial_x\partial_y + (1+h_x^2)\partial_y^2 - \frac{(1+h_y^2)h_{xx} - 2}{1}\right.$$

and D is a constant related to the surface diffusivity. Here we take

$$\psi = \mathcal{E} + \gamma\kappa + \omega(h), \qquad (12)$$

where $\mathcal{E}$ is the elastic energy density at the surface, $\gamma\kappa$ represent the surface energy, and $\omega(h)$ is the wetting energy. In the above, the elastic energy density is

$$\mathcal{E} = \frac{1}{2}\sigma_{ij}^F E_{ij}^F \ \text{ on } \ z = h(x,y,t), \qquad (13)$$

and the curvature of the film κ is given by

$$\kappa = -\frac{(1+h_y^2)h_{xx} - 2h_xh_yh_{xy} + (1+h_x^2)h_{yy}}{(1+h_x^2+h_y^2)^{3/2}}. \qquad (14)$$

The model for the wetting potential $\omega(h)$ comes from a surface energy which changes from one value for the substrate to another value in the film. Using a boundary-layer transition model for the surface energy in which the transition occurs over an interfacial width δ, the corresponding wetting potential is[20]

$$\omega(h) = \frac{-1}{\sqrt{1+|\nabla h|^2}}\frac{\Delta\gamma}{\pi}\frac{\delta}{\delta^2+h^2}, \qquad (15)$$

where

$$\Delta\gamma = \gamma_S - \gamma_F \qquad (16)$$

is the difference in the surface energies of the substrate and the film.

EVOLUTION EQUATION

The evolution equation as given in Eq. (10) is two dimensional, but requires the solution of the three-dimensional elasticity problem to determine $\mathcal{E}$. The understanding of island formation using this equation is limited in number of islands and scale due to numerical considerations. We derive here a self-contained two-dimensional evolution equation based on the wavelength of surface undulations being large compared to the characteristic film thickness. This formulation has the advantage of requiring only a two-dimensional computational domain.

We define

$$\alpha = \frac{H_0}{l} \ll 1, \tag{17}$$

where H_0 is the characteristic film thickness, and l is the characteristic length scale in (x,y). Then we use the following scalings:

$$h = \alpha H l,$$

$$x = lX,$$

$$y = lY,$$

$$t = \tau T,$$

$$\tau = \frac{l^4}{D\gamma},$$

$$l = \frac{\gamma}{\mathcal{E}_0}, \tag{18}$$

where the elastic energy density $\mathcal{E}_0$ is given by

$$\mathcal{E}_0 = 2\mu\epsilon^2\left(\frac{1+\nu}{1-\nu}\right). \tag{19}$$

In Ref. 26 we developed a systematic solution to the elasticity problem and evolution equation using an asymptotic series in α. At $\mathcal{O}(1)$ we obtain a self-contained evolution equation

$$\frac{\partial H}{\partial T} = \nabla^2\left[\tilde{\mathcal{E}}_1(H) - \nabla^2 H - \frac{r}{H^2}\right], \tag{20}$$

where the nonlocal elastic energy term $\tilde{\mathcal{E}}_1$ is given from Fourier transforms,

$$\tilde{\mathcal{E}}_1 = -E\mathcal{F}^{-1}[a\hat{H}], \tag{21}$$

where the Fourier transforms are defined as

$$\hat{H}(a_X, a_Y) = \mathcal{F}[H] = \frac{1}{(2\pi)^2}\int_{-\infty}^{\infty}\int_{-\infty}^{\infty} H(X,Y)\exp[i(a_X X + a_Y Y)]dX\,dY,$$

$$H(X,Y) = \mathcal{F}^{-1}[\hat{H}] = \int_{-\infty}^{\infty}\int_{-\infty}^{\infty} \hat{H}(a_X, a_Y)\exp[-i(a_X X + a_Y Y)]da_X\,da_Y,$$

with $a=\sqrt{a_X^2 + a_Y^2}$. In the above, the elastic interaction of film and substrate is measured by

$$E = \frac{2\mu^F(1+\nu^F)(1-\nu^S)}{(1-\nu^F)\mu^S}, \tag{24}$$

the strength of the wetting energy quantified by

$$r = \frac{\Delta\gamma\delta^*}{\pi\gamma}, \tag{25}$$

where

$$\delta^* = \frac{\delta}{l\alpha^3}, \tag{26}$$

is a scaled wetting layer thickness.

The thin-film evolution equation [Eq. (20)] contains the effects of surface diffusion, elasticity, surface energy, and wetting energy (for the detailed derivation see Ref. 26). The first term on the right contains the elastic energy. Without the thin-film approximation the evaluation of this term requires the solution of a three-dimensional elasticity problem. Here, with the thin-film approximation, we have determined a self-consistent approximate solution given by the nonlocal term [Eq. (21)]. The second term on the right is the effect of surface energy in the thin-film approximation, and finally the last term on the right is the thin-film wetting energy.

The thin-film equation can be used to determine the stability of planar films. To determine the stability of planar films of thickness $\overline{H}$, we consider a normal-mode perturbation with wave numbers a_X and a_Y,

$$H = \overline{H} + \hat{H}\ \exp(\sigma T + ia_X X + ia_Y Y). \tag{27}$$

We consider $\hat{H} \ll \overline{H}$, substitute Eq. (27) into Eq. (20), and linearize to obtain the characteristic equation,

$$\sigma = -a^4 + Ea^3 - \frac{2r}{\overline{H}^3}a^2. \tag{28}$$

The neutral stability boundary is given by

$$\overline{H}_s = \left[\frac{2r}{a(E-a)}\right]^{1/3}. \tag{29}$$

When $\overline{H} > \overline{H}_s$ the film is unstable, and when $\overline{H} < \overline{H}_s$ the film is stable. See Fig. 1 for plot of $\overline{H}_s$.

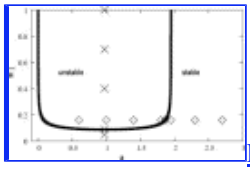

Figure 1.

From the characteristic equation we see that there is a critical film thickness $\overline{H}_c$, below which every film thickness is stable,

$$\overline{H}_c = \left(\frac{8r}{E^2}\right)^{1/3}, \qquad (30)$$

and there is a critical wave number a_c, above which every wave number is stable,

$$a_c = E. \qquad (31)$$

The evolution equation thus has the property that sufficiently thin films are stabilized by the wetting effect, but thicker films are unstable to the stress driven morphological instability.

NUMERICAL METHODS

In order to study the formation of islands in the region of instability, we have performed numerical simulation of Eq. (20) on a periodic domain $0 \leqslant X \leqslant L$ and $0 \leqslant Y \leqslant L$ by means of a pseudospectral method. In this approach we implement a variable-step predictor-corrector time integration. We use the difference between the predictor and the corrector as a measure of relative error at each step, and change the time step adaptively to ensure a local truncation error smaller than a prescribed tolerance. Define $a=2\pi/L$ and let

$$\hat{H}_{jk}(T) \equiv \mathcal{F}_{jk}(H) = \frac{1}{(2\pi)^2}\int_{-\infty}^{\infty}\int_{-\infty}^{\infty} H(X,Y,T)\exp\ i(jaX + kaY)dXdY,$$

where $\mathcal{F}_{jk}$ is the two-dimensional Fourier transform which we approximate by using the discrete Fourier transform (DFT),

$$\hat{H}_{jk} \simeq \hat{\mathcal{F}}_{jk}(H) = \frac{1}{nm}\sum_{p=0}^{n-1}\sum_{q=0}^{m-1} e^{i(jaX_p + kaY_q)} H(X_p, Y_q, T), \qquad (33)$$

where $X_p=pL/n$, $Y_q=qL/m$, $n=L/\Delta X$, and $m=L/\Delta Y$. We use the DFT to solve Eq. (20) in the frequency domain. Taking $\mathcal{F}_{jk}$ of Eq. (20) and using the DFT approximation, we obtain a system of evolution equations for the Fourier modes of the surface $\hat{H}_{jk}$,

$$\frac{\partial \hat{H}_{jk}}{\partial T} = -a_{jk}^4 \hat{H}_{jk} + E a_{jk}^3 \hat{H}_{jk} + a_{jk}^2 \hat{\omega}_{jk}, \qquad (34)$$

where

$$\hat{\omega}_{jk} = r\hat{\mathcal{F}}_{jk}(1/H^2), \qquad (35)$$

and

$$a_{jk} = a\sqrt{j^2 + k^2}. \qquad (36)$$

Equation (34) is linear except for $\hat{\omega}_{jk}$.

We solve Eq. (34) numerically and apply a predictor-corrector method. We use the explicit Euler method as predictor and for the corrector we use the second-order semi-implicit Adams-Bashforth method on the nonlinear part together with the fully implicit Adams-Bashforth method on the linear part. Hence using the predictor with the time step of size h we obtain the

predictor,

$$\hat{H}_{jk(p)}^{n+1} = \hat{H}_{jk}^{n} + h(-a_{jk}^{4}\hat{H}_{jk}^{n} + Ea_{jk}^{3}\hat{H}_{jk}^{n} + a_{jk}^{2}\hat{\omega}_{jk}^{n}), \quad (37)$$

from which we can find $\hat{\omega}_{jk(p)}^{n+1}$,

$$\hat{\omega}_{jk(p)}^{n+1} = r\hat{\mathcal{F}}_{jk}\left[\frac{1}{(H_{(p)}^{n+1})^2}\right]. \quad (38)$$

The corrector step is

$$\hat{H}_{jk}^{n+1} = \frac{1}{d}\left[\hat{H}_{jk}^{n} + \frac{h}{2}(-a_{jk}^{4}\hat{H}_{jk}^{n} + Ea_{jk}^{3}\hat{H}_{jk}^{n}) + \frac{h}{2}a_{jk}^{2}(\hat{\omega}_{jk(p)}^{n+1} + \hat{\omega}_{jk}^{n})\right], \quad (39)$$

where

$$d = 1 + \frac{h}{2}(a_{jk}^{4} - Ea_{jk}^{3}). \quad (40)$$

The second-order Adams-Bashforth method is locally second-order accurate in h.

We implement Eqs. (37),(38),(39) using a variable time step size and a fixed tolerance β. Starting with a large time step ΔT, we calculate ρ,

$$\rho \equiv \|H_{jk(p)} - H_{jk}\| = \sqrt{\frac{\sum_{j=1}^{n}\sum_{k=1}^{m}(H_{jk(p)} - H_{jk})^2}{nm}}, \quad (41)$$

which is the norm of the difference between the corrector and predictor. The result is accepted if $\rho \leqslant \beta$, otherwise rejected and recalculated using a smaller time step based on

$$\Delta T \to 0.9\Delta T\frac{\beta}{\rho}. \quad (42)$$

Equation (42) gives an adaptive scheme for which the local truncation error is bounded by a prescribed tolerance β. If ρ is small, $\rho<0.01\beta$, we increase the time step according to $\Delta T \to 2\Delta T$. The numerical method was validated on a number of test problems.[28]

RESULTS

To understand the nonlinear behavior of the thin-film equation we investigate the evolution of different initial conditions at the sample points indicated in Fig. 1 for both two-dimensional (2D) and three-dimensional (3D) initial conditions.

A.Two-dimensional initial condition

Here we use an initial condition corresponding to a sinusoidal ridge,

$$H = \overline{H} - H_0 \cos(AX). \qquad (43)$$

The parameters we used are E=1.9482 and r=3.1831×10^{-4} from Ge/Si materials,[26] and we implemented different choices of $\overline{H}$ and a in our code as shown in Fig. 1. Figure 2 shows a typical result for the evolution. After a transient period the solution converges in time to a steady state.

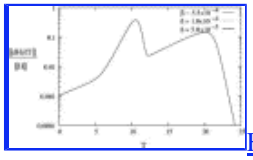
Figure 2.

Figure 3 shows the steady state island solution corresponding to the particular choice of the parameters. As we see from this result the valley we started with grows deeper but this growth stops when it gets to a sufficient depth.

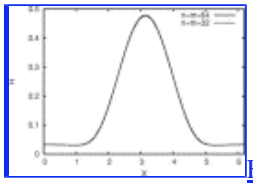
Figure 3.

The above result is specific to a choice of a and $\overline{H}$. To explore in more detail the shape of the islands using the numerical method, we fixed $\overline{H}$ and changed a as shown in Fig. 1. These results are shown in Fig. 4. The height of the islands decreases with decreasing domain size (increasing a). For a outside the stability boundary, from linear stability analysis (if $H_0 \ll \overline{H}$), we know that the steady state is a flat film. We confirmed this using our numerical method for a=E, a=2.3, and a=2.7 outside of the stability region. In fact the decay to the planar state occurs even for a large amplitude initial condition $\overline{H}$=0.16 and H_0=0.15. Finally, the point a=1.864 lies on $\overline{H}_s$. In this case as σ=0 we expect the initial island shape we started with neither to grow nor decay. Our numerical result also agrees with this.

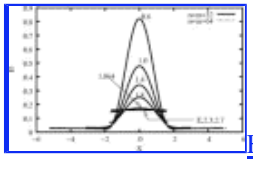
Figure 4.

To illustrate the effect of film thickness for fixed domain size we held a at E/2 and changed $\overline{H}$ as shown in Fig. 1. We obtained the results shown in Fig. 5. As the film gets thicker the height of the island gets larger for $\overline{H}$ in the instability region. In the stable region ($\overline{H}$=0.05) the initial ridge evolves to flat film.

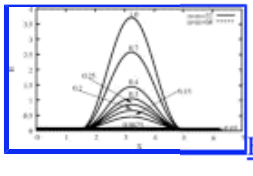
Figure 5.

Figures 6,7 summarize the above calculations in terms of the deviation of the final island shape from $\overline{H}$. In the case of fixed a, Fig. 6 shows that when we increase $\overline{H}$ the height of the island changes from flat to an island of positive height. In the case of fixed $\overline{H}$, Fig. 7 shows that as we increase the value of a, the island height decreases to a planar film.

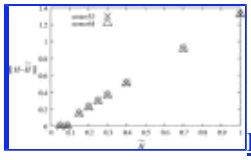
Figure 6.
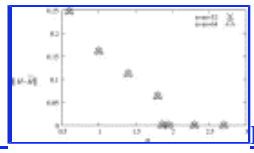
Figure 7.

B.Three-dimensional initial condition

For the 3D case we consider an initial condition of the doubly periodic sinusoid,

$$H = \overline{H} + 0.001\ \cos[(\sqrt{2}\pi/L)(X-Y)]\cos[(\sqrt{2}\pi/L)(X+Y) - \sqrt{2}\pi]. \quad (44)$$

We performed the same analysis as for the two-dimensional case for the parameters shown in Fig. 1.

Figures 8,9 show the steady state island solutions for fixed a and fixed $\overline{H}$, respectively. As we see from Fig. 8, as we increase $\overline{H}$ the island height increases. We also see from Fig. 9 that as a increases the island height decreases to a planar film. The first two figures in the bottom row of Fig. 9 behave as such because the wave number is close to the neutral stability criteria, the surface forms an interconnected periodic wavelike structure.

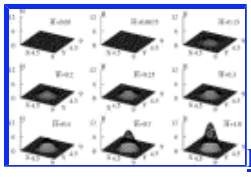
Figure 8.
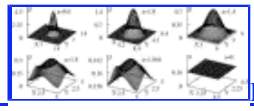
Figure 9.

Figures 10,11 show the deviation of the steady state island from the nominal film thickness $\overline{H}$. As we saw in Figs. 8,9, the steady state island height increases as $\overline{H}$ increases for a fixed a, and the steady state island height decreases as we increase a for fixed $\overline{H}$.

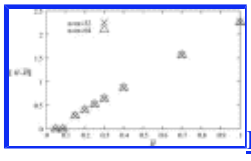
Figure 10.
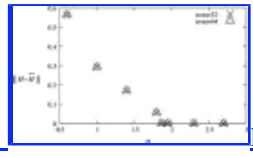
Figure 11.

Finally we implemented our numerical method on an initial condition of the form H=0.16+0.001A, where A is a random matrix generated using uniform distribution on [0,1]. The results obtained agree well with the two-dimensional and three-dimensional models we used above. Figure 12 shows a representative steady state solution from these calculations, illustrating that the convergence to a spatially periodic steady state solution is robust.

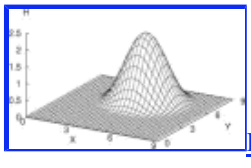
Figure 12.

SUMMARY

In this paper, we investigated the nonlinear steady state island solutions to the thin-film evolution equation for a strained film on a substrate. We developed a pseudospectral, predictor-corrector method for solving the evolution problem. Using this numerical method we showed that the evolution equation possesses steady state solutions corresponding to island formation. We characterized the family of equilibrium shapes in terms of the film thickness and the spatial periodicity for both two-dimensional (island ridge) and three-dimensional (quantum dot) morphologies.

ACKNOWLEDGMENTS

This research was supported by the National Science Foundation through a Nanoscale Interdisciplinary Research Team Grant (No. DMR-0102794).

REFERENCES

1. M. A. Kastner, in Proceedings of the 23rd International Conference on Physics of Semiconductors, Berlin, Germany, 1996, edited by M. Scheffler and R. Zimmerman (World Scientific, Singapore), Vol. 1, p. 27. first citation in article
2. M. Chen and W. Porod, J. Appl. Phys. **78**, 1050 (1995). [ISI] first citation in article
3. R. J. Asaro and W. A. Tiller, Metall. Trans. **3**, 1789 (1972). [ISI] first citation in article
4. M. A. Grinfeld, Dokl. Akad. Nauk SSSR **31**, 831 (1986) [Sov. Phys. Dokl. **31**, 831 (1986)]. [SPIN] first citation in article
5. D. J. Srolovitz, Acta Metall. **37**, 621 (1989). [Inspec] first citation in article
6. B. J. Spencer, P. W. Voorhees, and S. H. Davis, Phys. Rev. Lett. **67**, 3696 (1991). [MEDLINE] first citation in article
7. I. Daruka, J. Tersoff, and A. L. Barbasi, Phys. Rev. Lett. **82**, 2753 (1999). first citation in article
8. W. D. Nix, Metall. Trans. A **20A**, 2217 (1989). [Inspec] [ISI] first citation in article
9. H. Gao, J. Mech. Phys. Solids **39**, 443 (1991). [Inspec] [ISI] first citation in article
10. H. Gao, Int. J. Solids Struct. **28**, 703 (1991). first citation in article
11. M. A. Grinfeld, J. Nonlinear Sci. **3**, 35 (1993). first citation in article
12. J. Berrehar, C. Caroli, C. Lapersonne-Meyer, and M. Schott, Phys. Rev. B **46**, 13487 (1992). [ISI] [MEDLINE] first citation in article
13. D. E. Jesson, S. J. Pennycook, J. M. Baribeau, and D. C. Houghton, Phys. Rev. Lett. **71**, 1744 (1993). [MEDLINE] first citation in article
14. W. H. Yang and D. J. Srolovitz, J. Mech. Phys. Solids **42**, 1551 (1994). first citation in article
15. B. J. Spencer and D. I. Meiron, Acta Metall. Mater. **37**, 621 (1994). first citation in article
16. Y. Xiang and E. Weinan, J. Appl. Phys. **91**, 9414 (2002). [ISI] first citation in article
17. B. J. Spencer and J. Tersoff, Mater. Res. Soc. Symp. Proc. **399**, 283 (1996). first citation in article
18. B. J. Spencer and J. Tersoff, Phys. Rev. Lett. **79**, 4858 (1997). [ISI] first citation in article
19. R. V. Kukta and L. B. Freund, J. Mech. Phys. Solids **45**, 1835 (1997). [Inspec] [ISI] first citation in article
20. B. J. Spencer, Phys. Rev. B **59**, 2011 (1999). first citation in article
21. C. D. Rudin and B. J. Spencer, J. Appl. Phys. **86**, 5530 (1999). [ISI] first citation in article
22. L. L. Shanahan and B. J. Spencer, Interfaces Free Boundaries **4**, 1 (2002). [MathRev] first citation in article
23. Y. W. Zhang and A. F. Bower, J. Mech. Phys. Solids **47**, 2273 (1999). [Inspec] [ISI] first citation in article
24. P. Liu, Y. W. Zhang, and C. Lu, Phys. Rev. B **68**, 035402 (2003). [ISI] first citation in article
25. A. A. Golovin, S. H. Davis, and P. W. Voorhees, Phys. Rev. E **68**, 056203 (2003). [ISI] first citation in article
26. W. T. Tekalign and B. J. Spencer, J. Appl. Phys. **96**, 5505 (2004). [ISI] first citation in article
27. W. W. Mullins, J. Appl. Phys. **28**, 333 (1957). first citation in article
28. W. T. Tekalign, Ph.D. thesis, University at Buffalo, 2005. first citation in article
29. Y. Pang and R. Huang, Phys. Rev. B **74**, 075413 (2006). first citation in article
30. M. S. Levine, A. A. Golovin, S. H. Davis, and P. W. Voorhees, Phys. Rev. B **75**, 205312 (2007). first citation in article

FIGURES

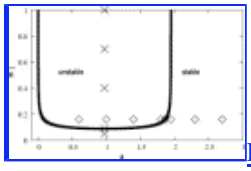
Full figure (10 kB)

Fig. 1. Stability boundary and sample points for simulations. First citation in article

---

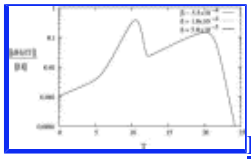
Full figure (10 kB)

Fig. 2. Transient evolution to a steady state. Shown is the norm of the rate of change in the solution for a=0.6, $\overline{H}$=0.16, and H_0=0.001. Convergence of the numerical method in ΔT is indicated by the overlap of results for different tolerance β.

First citation in article

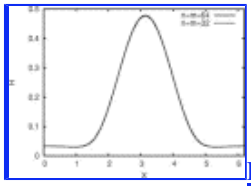
Full figure (11 kB)

Fig. 3. The 2D steady state solution for a=1.0, $\overline{H}$=0.16, and H_0=0.001. First citation in article

---

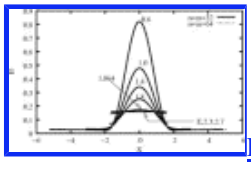
Full figure (13 kB)

Fig. 4. The 2D steady state solutions for fixed $\overline{H}$=0.16 and a=0.6, 1.0, 1.4, 1.8, 1.864, E, 2.3, and 2.7. First citation in article

---

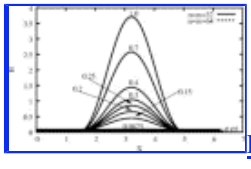
Full figure (15 kB)

Fig. 5. The 2D steady state solutions for fixed a=E/2 and $\overline{H}$=0.05, 0.0875, 0.15, 0.2, 0.25, 0.3, 0.4, 0.7, and 1.0. First citation in article

---

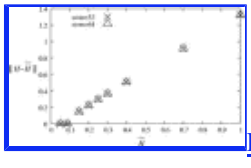
Full figure (9 kB)

Fig. 6. Summary of 2D steady states, $\|H-\overline{H}\|$ vs $\overline{H}$ fixing the value of a at E/2. First citation in article

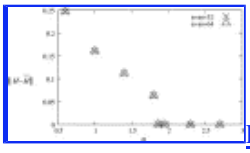
Full figure (8 kB)

Fig. 7. Summary of 2D steady states, $\|H-\overline{H}\|$ vs a fixing the value of $\overline{H}$ at 0.16. First citation in article

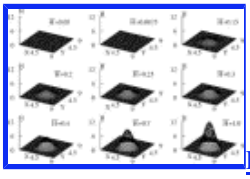
Full figure (27 kB)

Fig. 8. The 3D steady state solutions for fixed $a=E/2$ with $n=m=64$. First citation in article

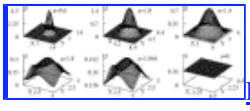
Full figure (19 kB)

Fig. 9. The 3D steady state solutions for fixed $\overline{H}=0.16$. Note the different x,y scalings in each plot. First citation in article

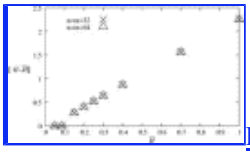
Full figure (8 kB)

Fig. 10. Summary of 3D steady states, $\|H-\overline{H}\|$ vs $\overline{H}$ fixing the value of a at $E/2$. First citation in article

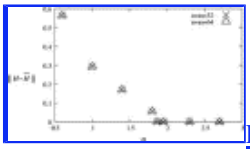
Full figure (7 kB)

Fig. 11. Summary of 3D steady states, $\|H-\overline{H}\|$ vs a fixing the value of $\overline{H}$ at 0.16. First citation in article

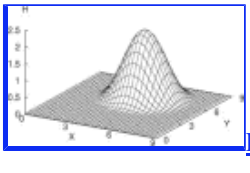
Full figure (16 kB)

Fig. 12. The steady state solution for a random initial condition ($n=m=32$). First citation in article

FOOTNOTES

*Electronic mail: wttsma@rit.edu

Up: Issue Table of Contents